

Report Documentation Page				Form Approved OMB No. 0704-0188	
Public reporting burden for the collection of information is estimated to average 1 hour per response, including the time for reviewing instructions, searching existing data sources, gathering and maintaining the data needed, and completing and reviewing the collection of information. Send comments regarding this burden estimate or any other aspect of this collection of information, including suggestions for reducing this burden, to Washington Headquarters Services, Directorate for Information Operations and Reports, 1215 Jefferson Davis Highway, Suite 1204, Arlington VA 22202-4302. Respondents should be aware that notwithstanding any other provision of law, no person shall be subject to a penalty for failing to comply with a collection of information if it does not display a currently valid OMB control number.					
1. REPORT DATE 04 JUN 2015		2. REPORT TYPE		3. DATES COVERED 00-00-2015 to 00-00-2015	
4. TITLE AND SUBTITLE A Parameter-Free Dynamic Alternative to Hyper-Viscosity for Coupled Transport Equations: Application to the Simulation of 3D Squall Lines Using Spectral Elements				5a. CONTRACT NUMBER	
				5b. GRANT NUMBER	
				5c. PROGRAM ELEMENT NUMBER	
6. AUTHOR(S)				5d. PROJECT NUMBER	
				5e. TASK NUMBER	
				5f. WORK UNIT NUMBER	
7. PERFORMING ORGANIZATION NAME(S) AND ADDRESS(ES) Naval Postgraduate School, Department of Applied Mathematics, Monterey, CA, 93943				8. PERFORMING ORGANIZATION REPORT NUMBER	
9. SPONSORING/MONITORING AGENCY NAME(S) AND ADDRESS(ES)				10. SPONSOR/MONITOR'S ACRONYM(S)	
				11. SPONSOR/MONITOR'S REPORT NUMBER(S)	
12. DISTRIBUTION/AVAILABILITY STATEMENT Approved for public release; distribution unlimited					
13. SUPPLEMENTARY NOTES					
14. ABSTRACT The stabilization of high order spectral elements to solve the transport equations for tracers in the atmosphere remains an active topic of research among atmospheric modelers. This paper builds on our previous work on variational multiscale stabilization (VMS) and discontinuity capturing (DC) [Variational multiscale stabilization of high-order spectral elements for the advection-diffusion equation J. Comput. Phys. 231 (2012) 7187-7213] and shows the applicability of VMS+DC to realistic atmospheric problems that involve physics coupling with phase change in the simulation of 3D deep convection. We show that the VMS+DC approach is a robust technique that can damp the high order modes characterizing the spectral element solution of complex coupled transport problems. The method has important properties that techniques of more common use often lack 1) it is free of a user-defined parameter, 2) it is anisotropic in that it only acts along the flow direction, 3) it is numerically consistent, and 4) it can improve the monotonicity of high-order spectral elements. The proposed method is assessed by comparing the results against those obtained with a fourth-order hyper-viscosity programmed in the same code. The main conclusion that arises is that tuning can be fully avoided without loss of accuracy if the dissipative scheme is properly designed. Finally, the cost of parallel communication is that of a second order operator which means that fewer communications are required by VMS+DC than by a hyper-viscosity method fewer communications translate into a faster and more scalable code, which is of vital importance as we approach the exascale range of computing.					
15. SUBJECT TERMS					
16. SECURITY CLASSIFICATION OF:			17. LIMITATION OF ABSTRACT Same as Report (SAR)	18. NUMBER OF PAGES 26	19a. NAME OF RESPONSIBLE PERSON
a. REPORT unclassified	b. ABSTRACT unclassified	c. THIS PAGE unclassified			

A Parameter-Free Dynamic Alternative to Hyper-Viscosity for Coupled Transport Equations: Application to the Simulation of 3D Squall Lines Using Spectral Elements

Simone Marras and Francis X. Giraldo

*Naval Postgraduate School
Department of Applied Mathematics
833 Dyer Rd., Spanagel SP249A, Monterey, CA 93943, US
smarras1@nps.edu, fxgirald@nps.edu*

Abstract

The stabilization of high order spectral elements to solve the transport equations for tracers in the atmosphere remains an active topic of research among atmospheric modelers. This paper builds on our previous work on variational multiscale stabilization (VMS) and discontinuity capturing (DC) [*Variational multiscale stabilization of high-order spectral elements for the advection-diffusion equation* J. Comput. Phys. 231 (2012) 7187-7213] and shows the applicability of VMS+DC to realistic atmospheric problems that involve physics coupling with phase change in the simulation of 3D deep convection. We show that the VMS+DC approach is a robust technique that can damp the high order modes characterizing the spectral element solution of complex coupled transport problems. The method has important properties that techniques of more common use often lack: 1) it is free of a user-defined parameter, 2) it is anisotropic in that it only acts along the flow direction, 3) it is numerically consistent, and 4) it can improve the monotonicity of high-order spectral elements. The proposed method is assessed by comparing the results against those obtained with a fourth-order hyper-viscosity programmed in the same code. The main conclusion that arises is that tuning can be fully avoided without loss of accuracy if the dissipative scheme is properly designed. Finally, the cost of parallel communication is that of a second order operator which means that fewer communications are required by VMS+DC than by a hyper-viscosity method; fewer communications translate into a faster and more scalable code, which is of vital importance as we approach the exascale range of computing.

Keywords: Residual-based Stabilization, Variational Multiscale Method, VMS, VMM, Crosswind Discontinuity Capturing, Dynamic Artificial Diffusion, Hyper-Viscosity, Spectral Element Method, Monotonicity-preserving High-order Methods, Stabilization of Spectral Elements, Deep Convection, Kessler Microphysics

1. Introduction

In the field of numerical weather prediction, regardless of the numerical method that atmospheric models use, dissipation of some sort is added for various reasons. Stabilization is one of them and represents the main topic of analysis of this paper. Due to its ease of implementation and robustness, artificial diffusion is the most common mean of dissipation that is found in current research and operational weather forecast models (cf. Jablonowski and Williamson (2011) and citations therein). Given an advection-dominated problem described by the general evolution equation

$$q_t = \mathcal{L}q, \quad (1)$$

where \mathcal{L} is a set of differential operators acting in space on q , the explicit dissipation of q is classically modeled as a diffusion operator (hyper-viscosity, HV, from now on) in the form of

$$HV = (-1)^{\alpha+1} \nabla^\alpha \cdot (\nu_{2\alpha} \nabla^\alpha q), \quad (2)$$

where α is a positive integer and $\nu_{2\alpha}$ is the diffusivity coefficient. HV is sometimes found also in other fields of computational fluid dynamics; one example is found in Baruzzi et al. (1992) to preserve higher order accuracy in the simulation of high speed flows. In the stabilization of finite elements, the orthogonal subscale (OSS) approach for sub-gridscale modeling (see, e.g., Codina (2002)) could, in principle, also be seen as a dynamic version of such a scheme. However, even if HV in the form of Eq. (2) is scale-selective and only damps higher frequencies, it is not physical. With respect to consistency, the diffusion coefficient should decrease as the grid is refined; this condition is respected by HV if the value of its coefficients is reduced as the resolution increases, approaching zero as the grid is sufficiently refined. Nonetheless, because HV does not depend on the residual of the equations, its strength and anisotropy cannot adapt to the flow direction and strength automatically. Additionally, for a stabilizing scheme to preserve the shape of the tracer, dissipation normal to the flow should be avoided whereas the dissipation in the direction of the flow should be sufficient to control instabilities or unboundedness (Hughes and Brooks, 1979; Hughes et al., 1986; Codina, 1993). This condition will not be respected by diffusion schemes such as HV, as exemplified in Fig. 1. To preserve the correct physical dimensions of the hyper-viscous term, the value of $\nu_{2\alpha}$ must scale correctly with respect to α and the grid spacing. Its selection not only is non-trivial, but has a great impact on the solution of the problem. Quoting Jablonowski and Williamson (2011) "The choice of the ∇^2 , ∇^4 or even higher-order diffusion coefficient is most often motivated by empirical arguments and chosen in a somewhat arbitrary manner. It is sometimes even considered a model tuning parameter [...]"

It is well known that the straightforward numerical approximation of Eq. (1) that models advection-dominated problems is characterized by Gibbs oscillations that may render the solution unacceptable. These oscillations are treated by either anti-aliasing filters (e.g., VandeVen (1991); Boyd (1998)) alone or, possibly, by a combination of the latter with some type of artificial diffusion in the form of (2) to improve the non-monotonic filtered solution. Research in finding the optimal solution to this problem is still ongoing (see, e.g., Malm et al. (2013)).

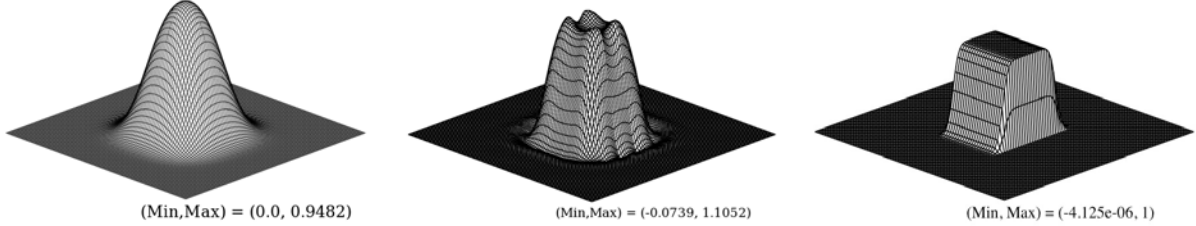


Figure 1: Advection of a 2D square wave in a doubly-periodic channel with velocity directed along the x -axis, which corresponds to the bottom-right edge of the squared surfaces in the three plots. Stabilization achieved by the operators ∇^2 (left) and ∇^4 (center), with constant coefficients $\nu_2 = 0.001 \text{ m}^2 \text{ s}^{-1}$ and $\nu_4 = 0.000001 \text{ m}^4 \text{ s}^{-1}$, respectively, and using VMS (right). Reprinted from Marras et al. (2012), Fig. 21, with permission from Elsevier.

In the quest for a solution to the drawbacks of HV and for the improvement of the monotonicity-preserving properties of stabilized high-order methods, the main novelty of our current paper lies in the application of the variational multiscale stabilization (VMS) by Hughes (1995) with the crosswind discontinuity capturing by Codina (1993) (DC from now on) to stabilize the spectral element solution of three coupled advection equations in the simulation of fully 3D deep convection. To our knowledge, the only application of VMS to high order spectral elements for coupled problems appears in Gjesdal et al. (2009) for the turbulence modeling of incompressible flows. In the case of Marras et al. (2012), VMS+DC was only applied to solve one scalar advection problem and verified against standard benchmarks in one and two dimensions. The characteristic velocities of deep convection may be orders of magnitude larger than those in the purely academic tests presented in our previous work, thereby subjecting the scheme to a more demanding test when it comes to stabilization and treatment of over- and undershoots. In the simulation of deep convection, this scheme was successfully applied by Marras et al. (2013) for 2D problems using linear finite elements. The main goal of this work is then to prove the applicability of VMS+DC to 3D realistic atmospheric simulations and show that VMS+DC is 1) parameter-free, 2) anisotropic, 3) numerically consistent, 4) inexpensive on parallel computers, and 5) can improve the monotonicity-preserving properties of high order spectral elements. We implement this stabilization method within the *Nonhydrostatic Unified Model of the Atmosphere* (NUMA) (Kelly and Giraldo, 2012; Giraldo et al., 2013).

The equation sets and the details of the residual-based stabilization and crosswind dissipation are reported in Sec. 2. The fundamental results for a fully 3D squall line simulation are shown in Sec. 3. A summary of our conclusions is discussed in Sec. 4.

2. Equations, their discretization, and stabilization techniques

Let $\Omega \in \mathbb{R}^3$ be a fixed three dimensional domain with boundary $\partial\Omega$ and Cartesian coordinates $\mathbf{x} = (x, y, z)$. Let us identify the dry air density, the velocity vector, and the potential temperature with the symbols ρ , \mathbf{u} , and θ . Let us also define the mixing ratios of water vapor, cloud water,

and rain as $q_v = \rho_v/\rho$, $q_c = \rho_c/\rho$ and $q_r = \rho_r/\rho$, where $\rho_{v,c,r}$ are the densities of water vapor, cloud, and rain. Furthermore, let $\rho'(t, \mathbf{x}) = \rho(t, \mathbf{x}) - \rho_0(z)$, $\theta'(t, \mathbf{x}) = \theta(t, \mathbf{x}) - \theta_0(z)$, and $p'(t, \mathbf{x}) = p(t, \mathbf{x}) - p_0(z)$ be the perturbations of density, potential temperature, and pressure with respect to a hydrostatically balanced background state indicated by the subscript 0 (see, e.g., Marchuk (1974)). Then, the strong form of the time-dependent Euler equations that model a stratified, moist atmosphere can be written as¹:

$$\begin{aligned}
\rho'_t + \mathbf{u} \cdot \nabla \rho + \rho \nabla \cdot \mathbf{u} &= 0, \\
\mathbf{u}_t + \mathbf{u} \cdot \nabla \mathbf{u} + \frac{1}{\rho} \nabla \cdot (\mathbf{I} p') &= g \mathbf{k} (1 + \epsilon q_v - q_c - q_r), \\
\theta'_t + \mathbf{u} \cdot \nabla \theta &= S_\theta(\rho, \theta, q_v, q_c, q_r), \\
q_{i_t} + \mathbf{u} \cdot \nabla q_i &= S_{q_i}(\rho, \theta, q_v, q_c, q_r), \quad \text{for } i = v, c, r,
\end{aligned} \tag{3}$$

where \mathbf{I} is the rank-3 identity matrix, $g \mathbf{k}$ is the acceleration of gravity directed as $\mathbf{k} = [001]^T$, and $\epsilon = R/R_v$ is the ratio of the gas constants of dry air, R , and of water vapor, R_v . θ , ρ , and p are related through the equation of state for a perfect gas. Because moist air contributes to the buoyancy of the flow, the right hand side of the momentum equation is corrected by the total buoyancy $\mathbf{B} = g \mathbf{k} (1 + \epsilon q_v - q_c - q_r)$. Due to the microphysical processes that involve phase change in the water content, the source/sink terms identified by S_{θ, q_i} are modeled and computed via the Kessler microphysics for warm clouds (Kessler, 1969). The system of Eqs. (3) must be solved in $\Omega \forall t \in (0, t_f)$ with properly assigned initial and boundary conditions. Because in this study we are mainly interested in the solution of the advection equations of water tracers, we concentrate on the last three equations of the system. To simplify the description of their numerical treatment later, we re-express them in compact form as:

$$\mathbf{q}_t + \mathcal{L} \mathbf{q} = \mathbf{S}(\mathbf{q}), \tag{4}$$

where

$$\mathbf{q} = \begin{bmatrix} q_v \\ q_c \\ q_r \end{bmatrix}, \quad \mathcal{L} \mathbf{q} = \mathbf{u} \cdot \nabla \begin{bmatrix} q_v \\ q_c \\ q_r \end{bmatrix}, \quad \mathbf{S}(\mathbf{q}) = \begin{bmatrix} S_{q_v} \\ S_{q_c} \\ S_{q_r} \end{bmatrix}. \tag{5}$$

Because the coupling of (4) with the Euler equations is done by the saturation adjustment of Soong and Ogura (1973), the solution is first obtained for the homogeneous counterpart of Eq. (4) before the sources are computed and the unknowns updated through `Kessler`. Because we

¹For the sake of precision, the Euler equations are only the first three equations of the system, and are coupled to the equations for the quantities q_i through velocity and the source terms.

already describe the spectral element approximation of the scalar counterpart of Eq. (4) in our previous work (Marras et al. (2012)), we can omit the details on spectral elements and proceed to the description of their stabilization.

2.1. Stabilization of spectral elements

Let us define the space of trial solutions as $\mathbf{Q} = \{\mathbf{q} \in \mathbf{H}^1(\Omega) : \mathbf{q} = g \text{ on } \partial\Omega\}$ and the space of test functions $\Psi = \{\psi \in H^1(\Omega) : \psi = 0 \text{ on } \partial\Omega\}$, where bold indicates a vector quantity and the discrete counterpart of \mathbf{Q} and Ψ will be indicated by the superscript h . Given the basis function ψ^h , the stabilized spectral element solution of (4) consists in finding the solution $\mathbf{q}^h \in \mathbf{Q}^h$ such that

$$\int_{\Omega^h} \psi^h [\mathbf{q}_t^h + \mathcal{L}\mathbf{q}^h] d\Omega^h + b(\psi^h, \mathbf{q}^h) = \int_{\Omega^h} \psi^h \mathbf{S}(\mathbf{q}) d\Omega^h \quad (6)$$

holds $\forall \psi^h \in \Psi^h$. In Eq. (6),

$$b(\psi^h, \mathbf{q}^h) = - \sum_{e=1}^{N_e} \int_{\Omega_e^h} [\mathcal{L}^* \psi^h] \tau \mathcal{R}(\mathbf{q}^h) d\Omega^h$$

is the stabilizing term defined as a function of: the adjoint operator \mathcal{L}^* acting onto the basis function, the equations residual $\mathcal{R}(\mathbf{q}^h)$, and the parameter

$$\tau = \left(\frac{2|\mathbf{u}|}{h} + \text{epsilon} \right)^{-1},$$

where h is a characteristic length of the computational grid. Because of the somewhat uncertain definition of τ (Knobloch (2008)), the choice of h may vary as a function of the physical characteristics of the problem and of the structure of the grid. For example, Owen et al. (2013) achieved better solutions by taking h as the length of the shortest element edge in the flow boundary layer. In this study we use $h = \sqrt{\Delta x^2 + \Delta y^2 + \Delta z^2}$, where $\Delta \cdot$ is the mean distance between two consecutive nodes within a high order element with unequally spaced nodes. Because velocity may be zero, the machine `epsilon` is added to avoid divisions by zero on the computer. Should it be the case that Eq. (4) included some physical diffusion ν (e.g. eddy viscosity, thermal diffusion), τ would simply include it in the form

$$\tau = \left(\frac{\nu}{h^2} + \frac{2|\mathbf{u}|}{h} + \text{epsilon} \right)^{-1}.$$

This is not the only definition of τ that can be found (see, e.g., Knobloch (2008)). For up to cubic elements with equally spaced nodes, a derivation of the components of τ was obtained by

Table 1: Recommended values of the constant C as a function of the elements' order.

	linear	quadratic	cubic	quartic
C	0.7	0.35	0.23	0.175

Houzeaux et al. (2009). Based on Houzeaux et al., τ for elements with unequally-spaced nodes was obtained by Marras et al. (2012) although, for the sake of simplicity and without a great loss of accuracy, it is not used in this study. Because $b(\psi^h, \mathbf{q}^h)$ is a function of the equation residual and of a characteristic grid size, the effect of stabilization goes to zero as the exact solution is approached. This makes the method numerically consistent. One additional property of this stabilizing scheme is its anisotropy. The stabilizing effect only acts along the direction of the flow, which is the only direction where advection dominates diffusion (if any).

2.2. Crosswind discontinuity capturing

Stabilization in the form of (6) is neither monotonic nor monotonicity preserving; hence, over- and undershoots are still likely to affect the solution. This is especially true for large gradients in the transported quantities. To overcome this issue for low order finite elements, Codina (1993) designed an additional controlled crosswind discontinuity capturing that acts in the proximity of internal and boundary layers and that is orthogonal to the wind direction. The additional dissipation to be added to Eq. (6) is built as

$$DC = \sum_{e=1}^{N_e} \int_{\Omega^h} \frac{1}{2} \max \left\{ 0, C - \frac{2\nu}{|\mathbf{u}_{||}|h} \right\} h \frac{|\mathcal{R}(q^h)|}{|\nabla q^h|} \nabla \psi^h \cdot \left(\mathbf{I} - \frac{\mathbf{u} \otimes \mathbf{u}}{|\mathbf{u}|^2} \right) \cdot \nabla q^h d\Omega^h, \quad (7)$$

where $\mathbf{u}_{||}$ is the velocity component in the streamline direction and \otimes indicates a tensor product. The constant C is not user-defined. Its values were suggested by Codina (1993) for linear and quadratic elements. Based on the values provided by Codina, we extend them to higher order polynomials by a simple extrapolation from the linear and quadratic values and report them in Table 1. Note that Codina assumes finite elements with equi-spaced nodes. Although the values that he suggests seem to conform sufficiently well with the Legendre-Gauss-Lobatto points at order 4, a proper study should be made to define C for higher order spectral elements. To our knowledge, this remains an open topic but falls beyond the scope of this paper. From now on, the symbol VMS+DC will be used to indicate stabilization with crosswind discontinuity capturing.

2.3. Anisotropic HV

Because of the large aspect ratio of the grid elements that we use in the three-dimensional cloud simulations presented below, where $h_{x,y} \gg h_z$, we implemented an anisotropic version of the hyper-viscosity operator defined in Eq. (2) and write it as

$$HV_a = (-1)^{\alpha+1} \nabla^\alpha \cdot (\bar{\nu}_{2\alpha} \nabla^\alpha q), \quad (8)$$

where

$$\bar{\bar{\nu}} = \begin{bmatrix} \nu_x & 0 & 0 \\ 0 & \nu_y & 0 \\ 0 & 0 & \nu_z \end{bmatrix}$$

is the matrix of the diffusion coefficients along the x, y and z directions. This scheme may be seen as a simplified version of the tensor hyper-viscosity that was recently analyzed in Guba et al. (2014). The implementation, albeit simple, requires some attention if the higher order operator is built recursively. After building the second order Laplace operator using Eq. (8), $\bar{\bar{\nu}}$ must be set to the identity matrix for every subsequent application of the higher order derivation.

Remark 1. The anisotropy of HV_a must be understood in a different way with respect to the anisotropy of VMS+DC. HV_a owes its anisotropy to the fact that the magnitude of the dissipation varies based on the shape of the grid but it still acts in all directions regardless of the flow features. On the other hand, VMS+DC is anisotropic in that the dissipation acts exclusively along the flow direction and not normal to it. This is an important feature that stabilizing schemes, unlike physical stresses or diffusion, should preserve to least affect the flow physics.

3. Numerical experiments

To verify that the NUMA implementation of the method is correct and able to reproduce the results of our previous work, we first run the *Atmo-3D* benchmark of Marras et al. (2012). The simulation of a fully three-dimensional squall line follows *Atmo-3D*. To understand how the method performs on moist dynamics, the negative values of the three moisture variables are not filtered in the Kessler microphysical scheme as is typically done to avoid negative moisture.

3.1. *Atmo-3D: cylindrical tracer in a buoyant atmosphere*

A passive tracer is transported in a neutrally stratified atmosphere contained in $\Omega = [1 \times \infty \times 1]$ km³. The simulation final time is $t_f = 600$ s. The neutral background atmosphere at uniform potential temperature $\theta_0 = 300$ K is perturbed by a cylindrical thermal of radius $r_c = 250$ m, centered in $(x_c, z_c) = (500, 350)$ m, aligned with the y -axis, and defined by

$$\theta' = \begin{cases} 0.5 \left[1 + \cos \left(\frac{r\pi}{r_c} \right) \right] & \text{if } r \leq r_c \\ 0 & \text{elsewhere,} \end{cases} \quad (9)$$

where $r = \sqrt{(x - x_c)^2 + (z - z_c)^2}$. The east, west, top, and bottom boundaries are modeled as free-slip solid walls whereas periodic boundary conditions are imposed on the north and south walls (y -direction).

The results plotted in Fig. 2 are quantitatively and qualitatively comparable to the simulations presented in our previous work where the element grids are defined by $10 \times 1 \times 10$ and $20 \times 1 \times 20$

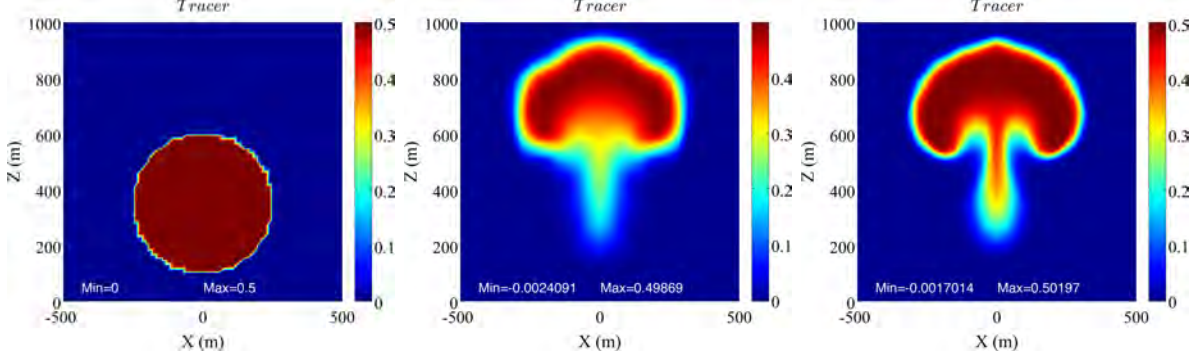


Figure 2: *Atmo-3D*: passive tracer in a rising thermal field. Vertical slice of q_{tracer} at $y = 0$ m. Left: initial condition. Center: coarse simulation with $10 \times 1 \times 10$ elements of order 4. Right: fine simulation with $20 \times 1 \times 20$ elements of order 4. The results are shown at time $t_f=600$ seconds.

elements of order 4. Nonetheless, a careful eye may spot minor differences. The differences are due to the use of different time-integrators between the two codes, which implies different time steps. The velocity field that drives the passive tracer is obtained by the coupling of the advection equations with the Euler equations that model the motion of the thermal bubble. To preserve a numerically stable SEM solution of the Euler equations, the Boyd-Vandeven filter (Vandeven, 1991; Boyd, 1998) was applied. Because this filter is not idempotent, its application at different time steps will give different solutions of thermal perturbation and, consequently, affect the solution of the water tracers. However, the results between the two model simulations are sufficiently similar which gives us confidence that the implementation of VMS+DC in NUMA is coded properly. We would like to stress that no filter was applied to the spectral element solution of the advection equations for the three tracers, that were solely stabilized by VMS and DC. We now proceed and verify the methodology in a fully coupled and convection-permitting system where the tracers are subjected to phase change and the equations are thermodynamically coupled to the Euler equations of compressible flows.

3.2. Squall line

To further evaluate VMS+DC we apply it to the simulation of (I) the squall line of Weisman et al. (1988) (WKR88, from now on) and of (II) the squall line over a flat terrain of Frame and Markowski (2006) (FM06, from now on). The two simulations are initialized with the same sounding given by Weisman and Klemp (1982) but differ in the domain size and in the intensity of the thermal perturbation. A westerly sheared flow has an increasing velocity ranging from 0 m s^{-1} at the surface to 17.5 m s^{-1} at $z = 2.5 \text{ km}$ and upward. We consider it useful to execute both simulations to test the sensitivity of the parameter-free scheme in different, yet similar, situations. Convection is triggered by a cylindrical thermal aligned with the y -axis and defined as

$$\theta' = \begin{cases} \theta_c \cos\left(\frac{r\pi}{2}\right)^2 + 0.5 \left| \sin\left(\frac{y\pi}{10}\right) + \cos(y2^{0.3}) \right| & \text{if } r \leq 1, \\ 0 & \text{elsewhere,} \end{cases} \quad (10)$$

where $r = \sqrt{(x - x_c)^2/r_x^2 + (z - z_c)^2/r_z^2}$, $\theta_c = 2$ K in WKR88, and $\theta_c = 4$ K in FM06. In both cases, the thermal has radii $(r_x, r_z) = (10 \text{ km}, 1.4 \text{ km})$ and is centered in the middle of the domain at (x_c, y_c, z_c) . The last two terms on the right hand side of Eq. (10) define a non-periodic perturbation to the otherwise axisymmetric thermal. We use this expression instead of a random perturbation of θ for the sake of reproducibility of the same initial state. At the four lateral boundaries periodicity is used, whereas the ground and top boundaries are modeled as inviscid solid surfaces. To absorb the vertically propagating gravity waves we add a 5 km absorbing sponge at $z = z_s = 12 \text{ km}$. The sponge is a Rayleigh-like layer defined as follows. In the area occupied by the sponge, the solution variables \mathbf{q} are corrected as $\mathbf{q} = \mathcal{D}(\mathbf{q} - \mathbf{q}_b)$, where b indicates the value of \mathbf{q} on the physical boundary and \mathcal{D} is the damping coefficient given by

$$\mathcal{D} = \begin{cases} \sin^4 \left[\frac{\pi}{2} \frac{(z - z_s)}{(z_{top} - z_s)} \right] & \text{if } z \geq z_s \\ 0 & \text{if } z < z_s. \end{cases}$$

3.2.1. Squall line I: WKR88

For the WKR88 test, we divide the domain $\Omega = [180 \times 120 \times 17.5] \text{ km}^3$ into $36 \times 16 \times 20$ elements of order 4. The simulation is executed until $t_f = 14400$ seconds. Without coefficients to be selected, only one simulation is executed using VMS+DC. On the other hand, four simulations are run using hyper-diffusion: a first set of three using HV with uniform coefficients $\nu_4 = \{10^4, 10^6, 10^8\} \text{ m}^4 \text{ s}^{-1}$ and one using HV_a with coefficients $\nu_x = \nu_y = 1 \times 10^7 \text{ m}^4 \text{ s}^{-1}, \nu_z = 3 \times 10^4 \text{ m}^4 \text{ s}^{-1}$. As we will notice below, these values of ν_x, ν_y and ν_z would make the simulation unstable if used isotropically. The time series of maximum and minimum vertical velocities are plotted in Fig. 3. For all the diffusion configurations the first updraft is triggered within the first 30 minutes. In the case of VMS+DC, peak values between 35 and 45 m s^{-1} are reasonably comparable to the observed 30 m s^{-1} of Weisman et al. (1988) for the same 17.5 m s^{-1} shear. The absolute value and trend are also in agreement with Weisman and Klemp (1982) where a sequence of storm growths and declines are observed due to the continuous cycle of cloud formation, rainout, and dissipation. A steadily decreasing intensity of the updrafts is predicted by all the HV solutions as well, although the maximum strength of the updrafts larger than 60 m s^{-1} is possibly indicating that none of the HV coefficients selected so far is sufficiently dissipative under these flow conditions. Albeit educated, the choice of ν_4 is practically arbitrary. Of these three values, the only ν_4 that preserves stability for the full length of the 14400 second simulation is $\nu_4 = 1 \times 10^6 \text{ m}^4 \text{ s}^{-1}$, even if the large 85 m s^{-1} peak at approximately 2.5 hours and another large peak at almost 4 hours are the symptoms of an incipient breaking that was eventually controlled by the end of the simulation. Given the current grid, the other values of ν_4 are either too small or too large and hence cause the simulation to lose stability. In simple words, when ν_4 is too small, the stability loss is due to the insufficient dissipation at the

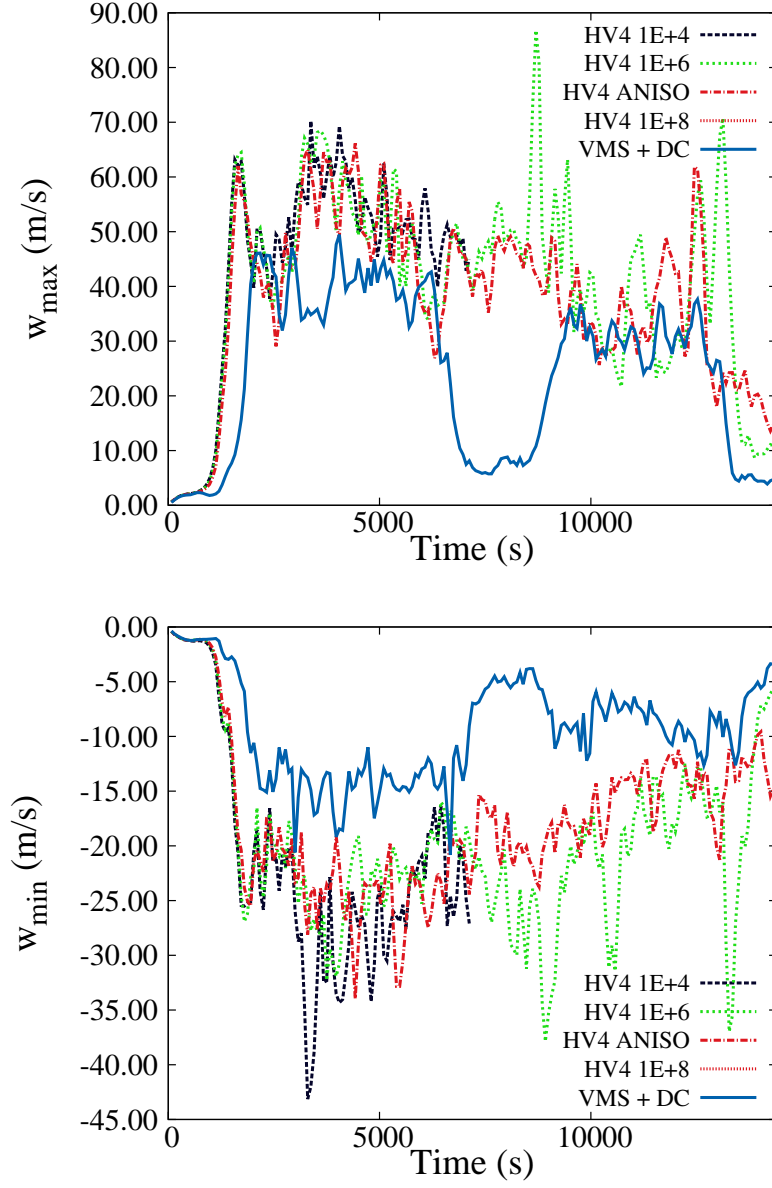


Figure 3: WKR88: time evolution of $\max(w)$ (top) and $\min(w)$ (bottom). Because the HV simulation with $\nu_4 = 1 \times 10^8 \text{ m}^4 \text{ s}^{-1}$ lost stability within the very first seconds, its time series are not visible in the plots. This is also reflected in the curves of q_c and q_r in Fig. 4.

given resolution. The value $\nu_4 = 1 \times 10^4 \text{ m}^4 \text{ s}^{-1}$ preserves a stable simulation for approximately 2 hours but breaks right after, as visible from the trimmed black curve in Fig. 3. The problem can be solved by either increasing the resolution or increasing the dissipation coefficient. In either case, the time step must be decreased to respect the stringent limit that diffusion and resolution impose on the time step. Although we are using an implicit-explicit (IMEX) time integration scheme to solve the system of equations (3), diffusion is currently treated explicitly. Diffusion may be included in the IMEX time-integrators but it would prevent us from deriving a Schur form, which is the reason for the success of IMEX methods. Because it falls beyond the scope of this paper, we will not enter the details of time integration and its analysis; the interested reader should refer to Giraldo et al. (2013) for more on this topic.

We are aware that we cannot increase ν_4 arbitrarily in this simulation because of the highly anisotropic grid made of elements that are much smaller along the z -direction than they are along x and y . Based on scaling arguments, this simply translates to choosing a smaller viscosity along z but still satisfying the larger dissipation needs in the two other directions. We then execute the simulation using the HV_a (Eq. (8)) with coefficients $\nu_x = \nu_y = 1 \times 10^7 \text{ m}^4 \text{ s}^{-1}$, $\nu_z = 3 \times 10^4 \text{ m}^4 \text{ s}^{-1}$ to reach a stable solution that admits maximum updrafts within the acceptable limits presented in previous studies. Improved results obtained with HV_a with respect to HV are noticeable by looking at the red, dashed-dotted curve in Fig. 3.

With respect to the treatment of the undershoots, Fig. 4 shows that VMS+DC greatly reduces the undershoots that affect cloud water and rain and that are not controlled by any of the 4th-order hyper-viscosities. To verify that the curtailing of the undershoots is not the mere result of excessive dissipation by VMS+DC, we plot the evolution of the total accumulated rainfall at 3600 s, 4800 s, and 7200 s in Fig. 5. Because Weisman et al. (1988) do not report the values of either accumulated or instantaneous precipitation, we refer to the values of total accumulated rainfall reported by Frame and Markowski (2006). In spite of the different domain and resolution, the values of Frame and Markowski are still a valuable source of expected precipitation given a certain initial sounding. In Frame and Markowski (2006), after 18000 s the precipitation ranges between 5 and 50 mm. In this study, at 7200 s the accumulated rainfall ranges between 0 and 35 mm (Fig. 5) and reaches a maximum of 60 mm after 14400 s (not shown). We should note that by 14400 s our squall line has crossed the western boundary and has re-entered the domain through the eastern boundary due to periodicity. For this reason, a direct comparison may be no longer possible since, at the second pass of the storm, more rain has precipitated in a region where it would have not precipitated otherwise. The contours of the accumulated rain from the HV_a simulation are plotted in the same figure. As partially expected from the observations of the time evolution of velocity, q_c , and q_r , the extremely small dissipative effect of HV_a causes a lot more rain to form and precipitate. Again, this is classically solved by better tuning the coefficients.

In Fig. 6, we show a vertical cross section of the line-averaged cloud content resolved by VMS+DC and HV. In agreement with the time series, as time evolves from 1800 to 7200 seconds the VMS+DC solution preserves stability and smoothness of the cloud water content. The classical anvil shape of the cloud is preserved by both simulations, although the HV solution presents an

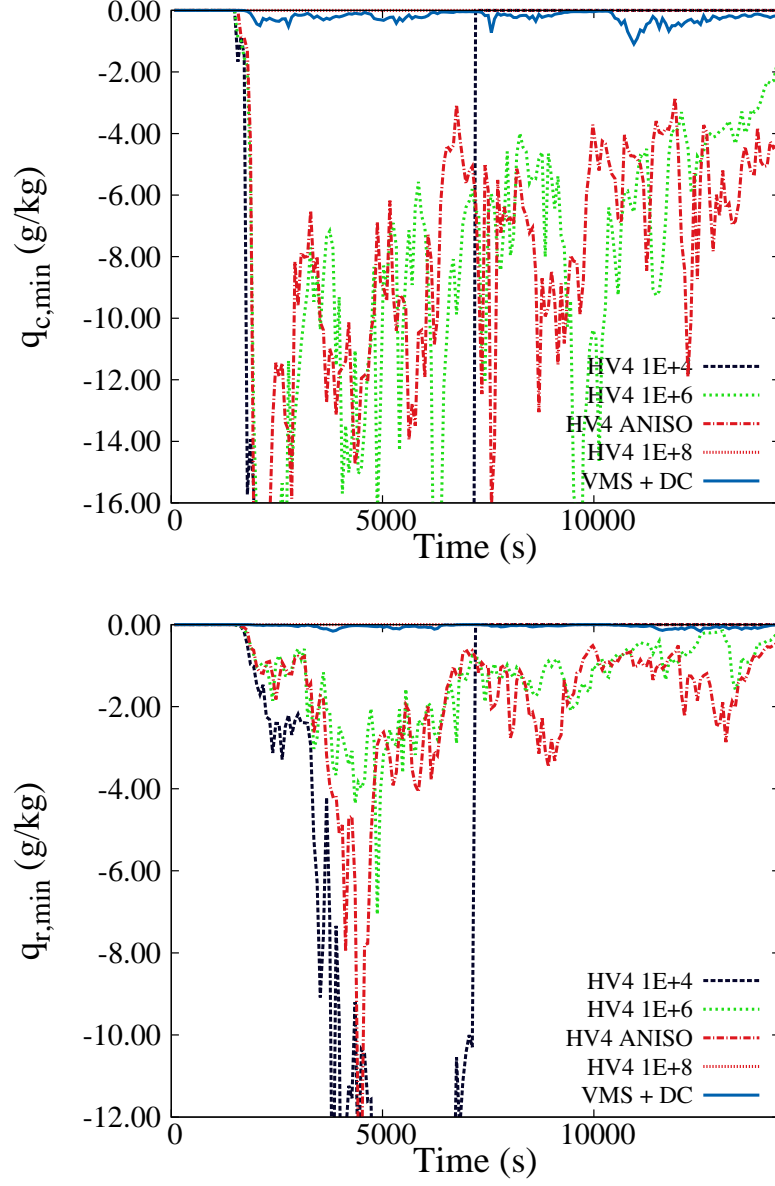


Figure 4: WKR88: time evolution of $\min(q_c)$ (top) and $\min(q_r)$ (bottom). Because the HV simulation with $\nu_4 = 1 \times 10^8 \text{ m}^4 \text{ s}^{-1}$ lost stability within the very first seconds, its time series is not visible in the plots.

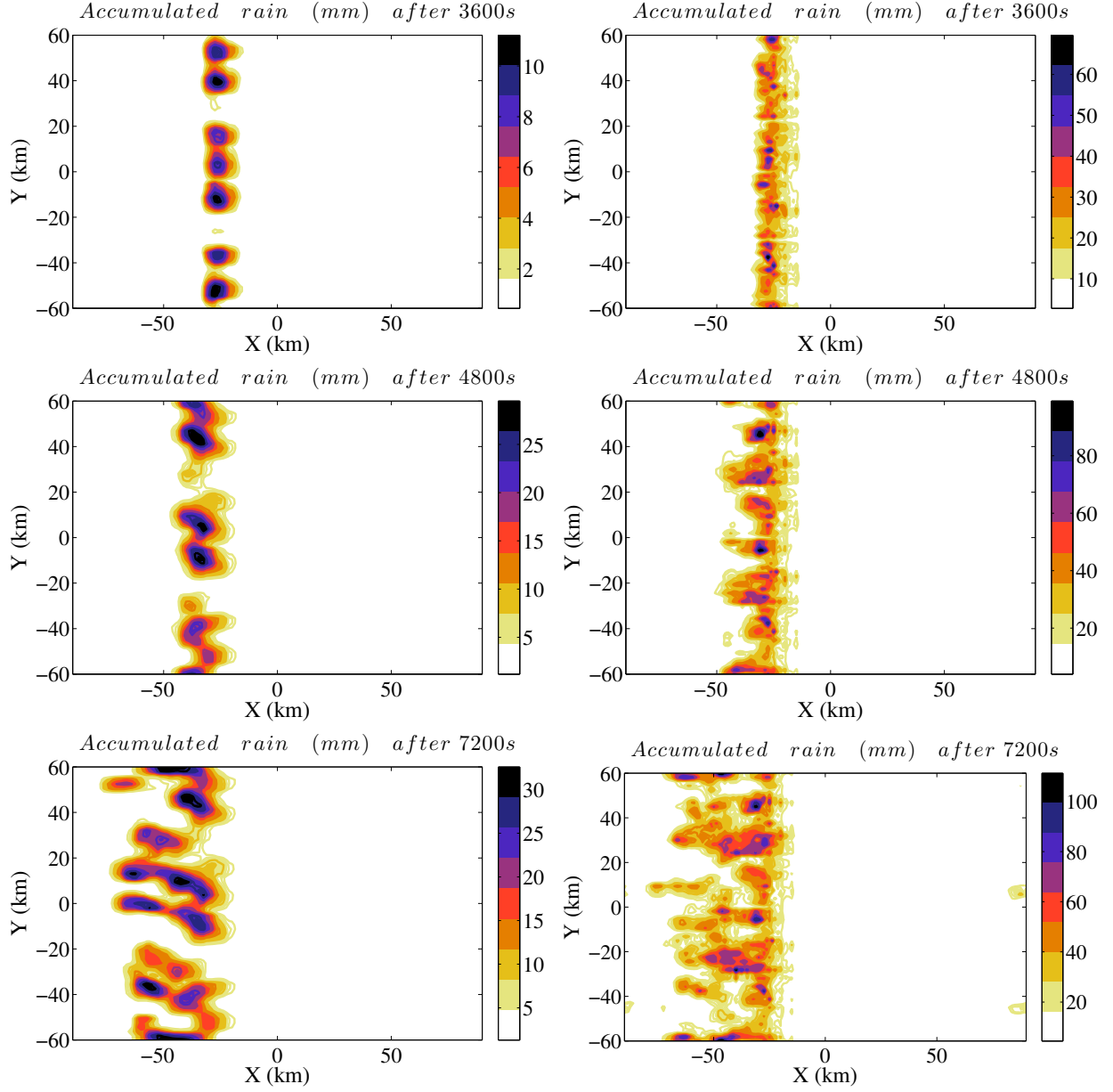


Figure 5: WKR88: total accumulated rainfall (mm) at $t_f = 3600s$ (top row), $t_f = 4800s$ (middle row), and $t_f = 7200s$ (bottom row). Left column: VMS+DC. Right column: HV_a with $\nu_x = \nu_y = 1 \times 10^7 \text{ m}^4 \text{ s}^{-1}$, $\nu_z = 3 \times 10^4 \text{ m}^4 \text{ s}^{-1}$.

overall increasing oscillatory behavior that eventually breaks the anvil and the overall shape of the cloud. This is simply due to the suboptimal choice of the diffusion coefficient. The same occurs with HV_a as is visible in the time series. The large extrema in the time series indicate that this particular HV simulation is close to diverging and that a slightly larger coefficient will improve the solution.

Remark 2. Throughout this article we often give hints on the possible solutions that could improve either HV or HV_a , but we limit ourselves to find the first possible coefficient that avoid the simulation to diverge. We never go further than this because the purpose of this article is not that of assessing HV, as this has been done thoroughly by other authors before. However, we still consider it necessary to show the results obtained with HV and HV_a to have a direct form of comparison of what can be achieved with VMS+DC when HV is coded in the same exact code and the same simulations are run. No conclusive remarks on HV are meant to arise from this analysis.

In Fig. 7 we are looking at the time and space evolution of the 3D iso-surfaces of q_c . The geometry, the position of the lifting condensation level, and the vertical extension of q_c obtained with VMS+DC are in good agreement with Weisman et al. (1988) and Weisman and Rotunno (2004). Since an analytic solution to this problem does not exist, we cannot draw definitive conclusions; however, given the specific initial sounding, certain properties of the space distribution of the storm should be consistent with previous studies, and we have been able to achieve this with VMS+DC. A first conclusion can already be drawn at this stage: without a constant to be tuned, VMS+DC can still produce suitable solutions. If we count the number of simulations that was necessary to run before obtaining a meaningful result from a parameter-dependent method, the enormous advantage of a parameter-free scheme is evident.

Given the same initial field but a different domain and different resolution, we then proceed with the FM06 test for further testing that may confirm this statement.

3.2.2. Squall line II: FM06

For the FM06 test, we divide the domain $\Omega=[300 \times 60 \times 17.5]$ km³ into $80 \times 12 \times 9$ elements of order 4. Our domain extends 100 km less than the FM06 along the x -axis. This makes the simulation relatively smaller but without compromising the full development of the physical features of the squall line. Periodic boundary conditions are used at the four lateral boundaries (unlike in Frame and Markowski (2006), where periodicity is imposed along y only). The simulation is run until $t_f = 18000$ seconds. We execute the same simulation using VMS+DC, isotropic HV with $\nu_4 = \{10^4, 10^6, 10^8\}$ m⁴s⁻¹, and HV_a with $\nu_x = \nu_y = 10^9$, $\nu_z = 3 \times 10^5$ m⁴s⁻¹.

The initial convection forms within the first 900 s for all cases; a line of single convective cells has formed by 1800 s and continues to develop while merging into one single line as the simulation continues (Fig. 8). The same features of the evolving storm are observed for VMS+DC and for every stable HV, including HV_a . This is stressed by the time series of the maximum and minimum vertical velocities plotted in Fig. 9. Except for $\nu_4 = 1 \times 10^4$ m⁴s⁻¹ and $\nu_4 = 1 \times 10^6$ m⁴s⁻¹, the maximum vertical velocities obtained with VMS+DC, HV with $\nu_4 = 1 \times 10^8$ m⁴s⁻¹, and HV_a show

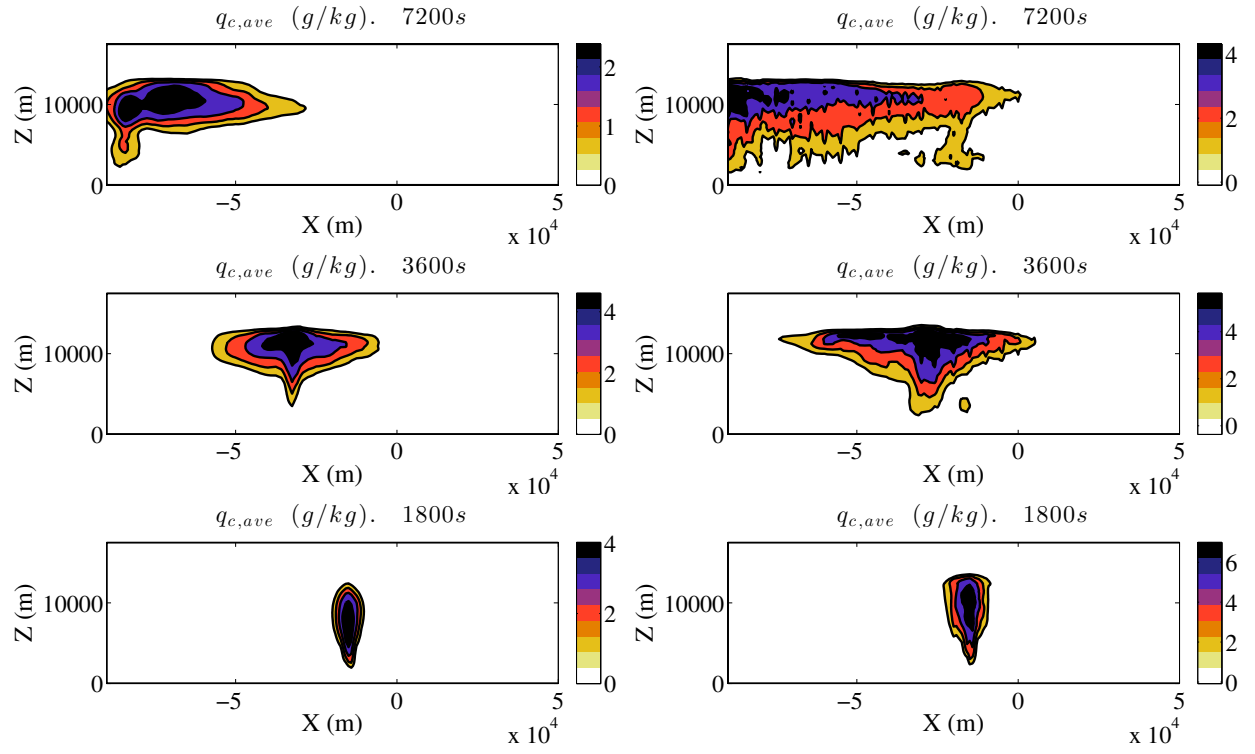


Figure 6: WKR88: line averaged vertical cross sections of q_c at 1800, 3600, and 7200 seconds. Stabilization achieved by VMS+DC (left column) and by HV with $\nu_4 = 1 \times 10^6 \text{ m}^4 \text{ s}^{-1}$ (right column).

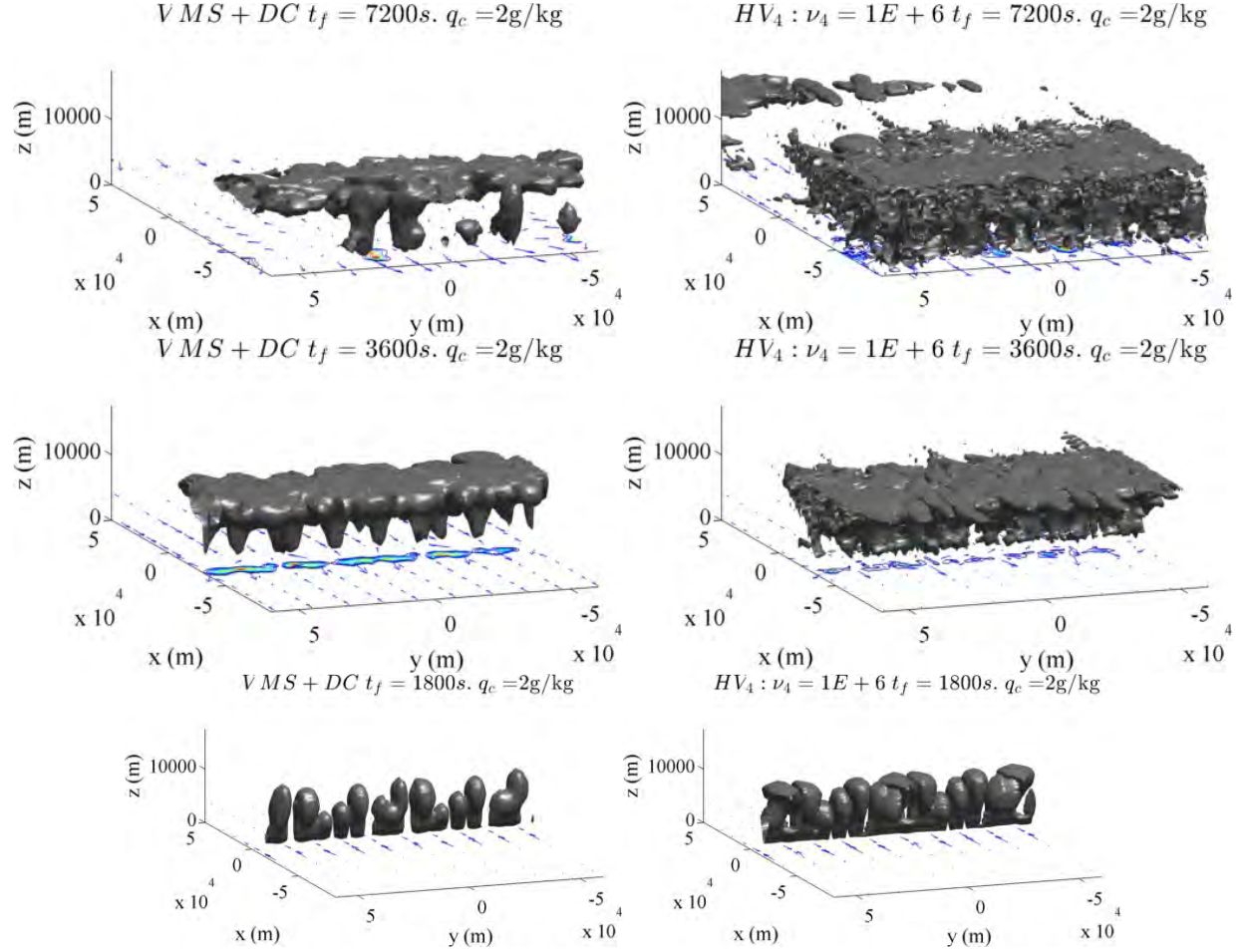


Figure 7: WKR88: perspective view of the squall line (grey scale) at 1800, 3600, and 7200 seconds. Stabilization achieved by VMS+DC (left column) and by HV with $\nu_4 = 1 \times 10^6 \text{ m}^4 \text{ s}^{-1}$ (right column). The velocity vectors at the surface are plotted every 7 grid points. The instantaneous surface rainfall is represented by the contour lines. The plotted domain is $\Omega_{plot} = 180 \times 120 \times 17.5 \text{ km}^3$. (In Matlab: azimuth = -110, elevation = 10).

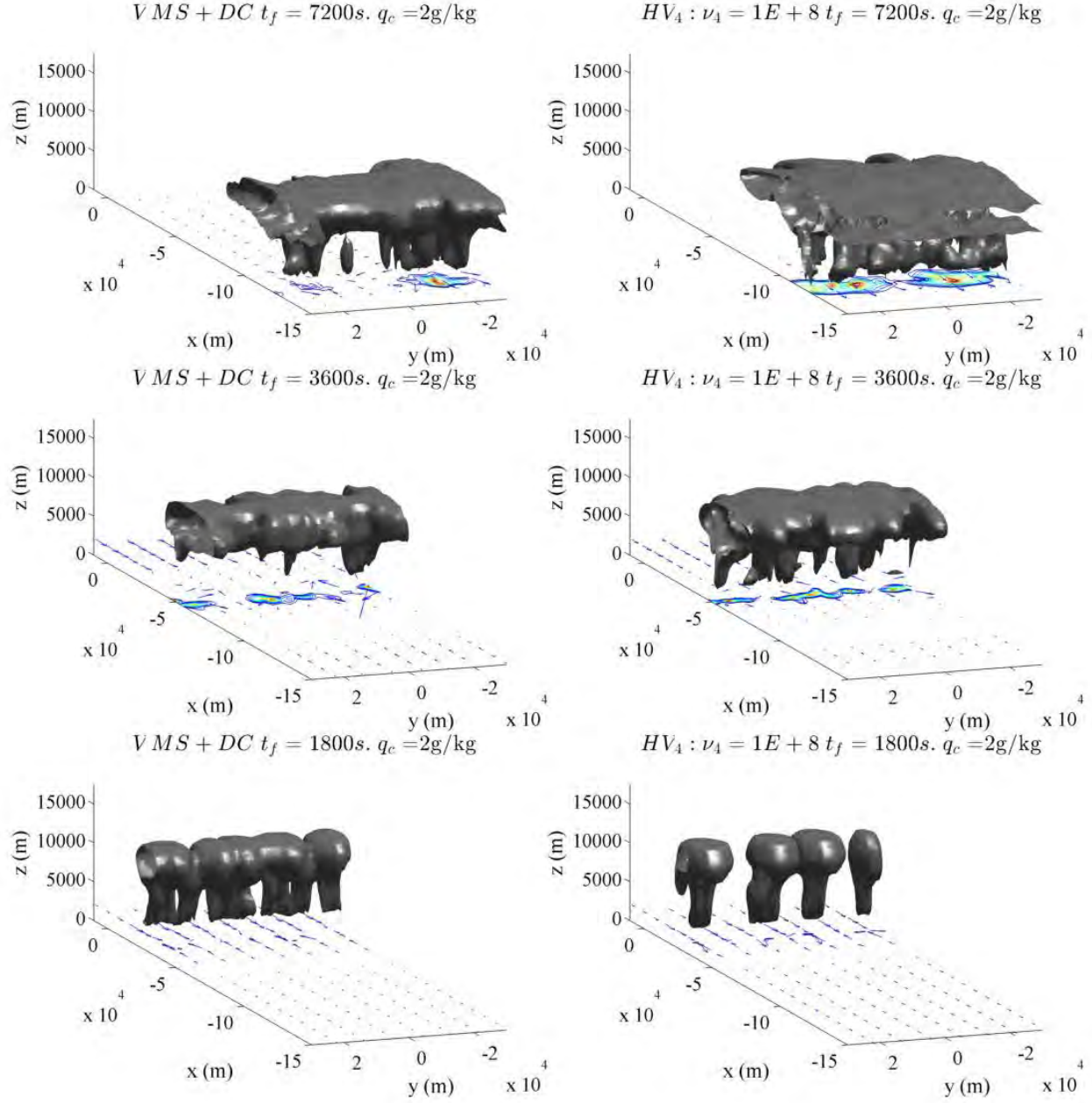


Figure 8: FM06: perspective view of the squall line (grey scale) at 1800, 3600, and 7200 seconds. Stabilization achieved by VMS+DC (left column) and by HV with $\nu_4 = 1 \times 10^8 \text{ m}^4 \text{ s}^{-1}$ (right column). The velocity vectors at the surface are plotted at every 7 grid points. The instantaneous surface rainfall is represented by the contour lines. The plotted domain is $\Omega_{plot} = 300 \times 60 \times 17.5 \text{ km}^3$. (In Matlab: azimuth = -110, elevation = 10).

the same rate of decay and extremely close values along the whole 18000 s. The absolute values and the trends are congruent with the literature².

Looking at the curves of $\min(q_c)$ and $\min(q_r)$ in Fig. 10, we see that our method is consistently controlling the undershoots of the tracers. It is interesting, however, to notice how the gap between VMS+DC and any HV for the current test is no longer as pronounced as it was for *Squall line I* (Fig. 4). We may have found the proper tuning of the HV coefficients that greatly limit $\min(q_r)$, although it still does not limit $\min(q_c)$.

The line-averaged contours of the cloud content are plotted in Fig. 11. As expected by looking at the time series, the VMS+DC and HV solutions are similar, with a relatively small difference in the value of q_c . The overall shape (characteristic anvil), the height of the lifting condensation level, and the vertical extension of q_c agree with Weisman et al. (1988) and Weisman and Rotunno (2004) for both solutions. The amount of accumulated rain confirms the similarities. We see this in Fig. 12 where the contours of total accumulated rainfall are plotted at $t_f = 18000$ s. We notice that the structure of the precipitation resolved by our method does not resemble the shape of the squall line as much as it did in Fig. 5. Nevertheless, the irregular pattern is supported by Frame and Markowski (2006), although with a difference of a few millimeters in the maximum value of precipitated water in both VMS+DC and HV_a.

4. Conclusions

We have presented a dynamic and parameter-free alternative to the classical fourth order hyper-viscosity to stabilize the solution of the coupled transport equations of water tracers to simulate 3D deep convection using spectral elements. The current method, based on the Variational Multiscale Stabilization (VMS) with crosswind discontinuity capturing (DC), has shown to have certain important properties that make it a suitable stabilizing alternative to hyper-viscosity in the simulation of atmospheric problems modeled by a system of coupled transport equations with phase change. Most importantly, VMS+DC is parameter-free –a clear advantage from the point of view of the user of the code; it is numerically consistent; and it is anisotropic. Furthermore, it improves the positivity preserving properties of the spectral element solution of the advection problem without the need for additional filters. In the simulation of moist convection, this property is of major importance although it remains a challenge to construct positivity preserving schemes at higher order (e.g., see Marras et al. (2012) for one possibility of tackling this problem). Although our approach is not fully monotonicity preserving (at least not for spectral element basis functions beyond second order), it still helps in minimizing the undershoots. Obtaining negative tracers is of major concern in weather simulations and climate modeling. With respect to parallel efficiency, because each Laplacian requires one communication, fewer communications are required by VMS

²Because Frame and Markowski (2006) do not provide this information, we rely on a comparison with Weisman et al. (1988) and Weisman and Rotunno (2004) whose initial state is the same.

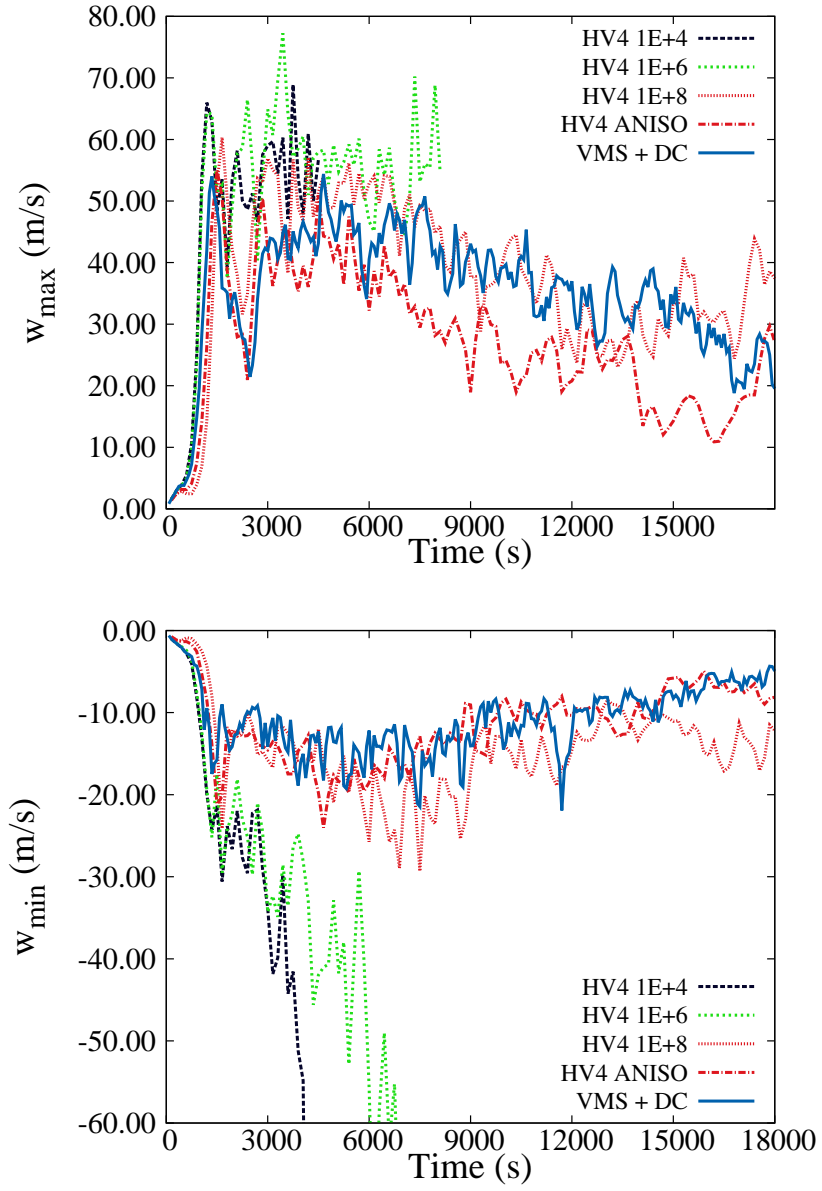


Figure 9: FM06: Time evolution of $\max(w)$ (top) and $\min(w)$ (bottom).

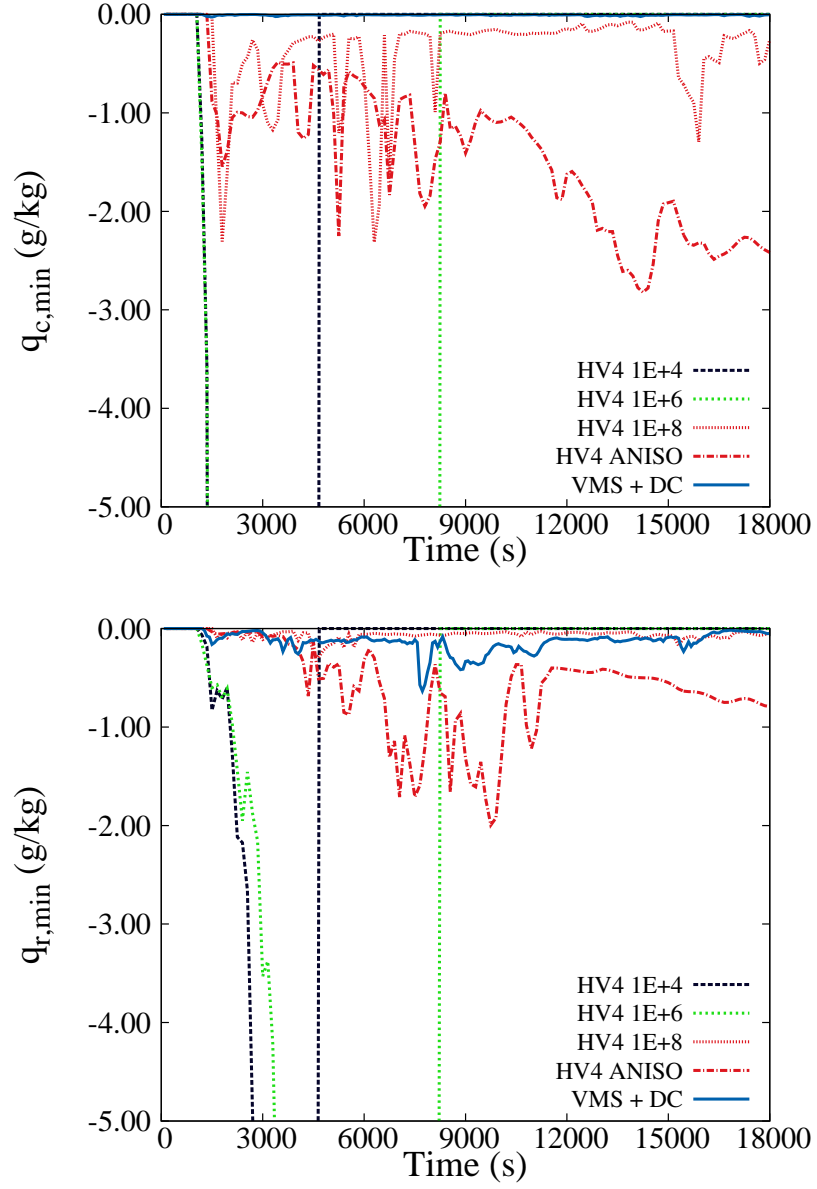


Figure 10: FM06: time evolution of $\min(q_c)$ (top) and $\min(q_r)$ (bottom)

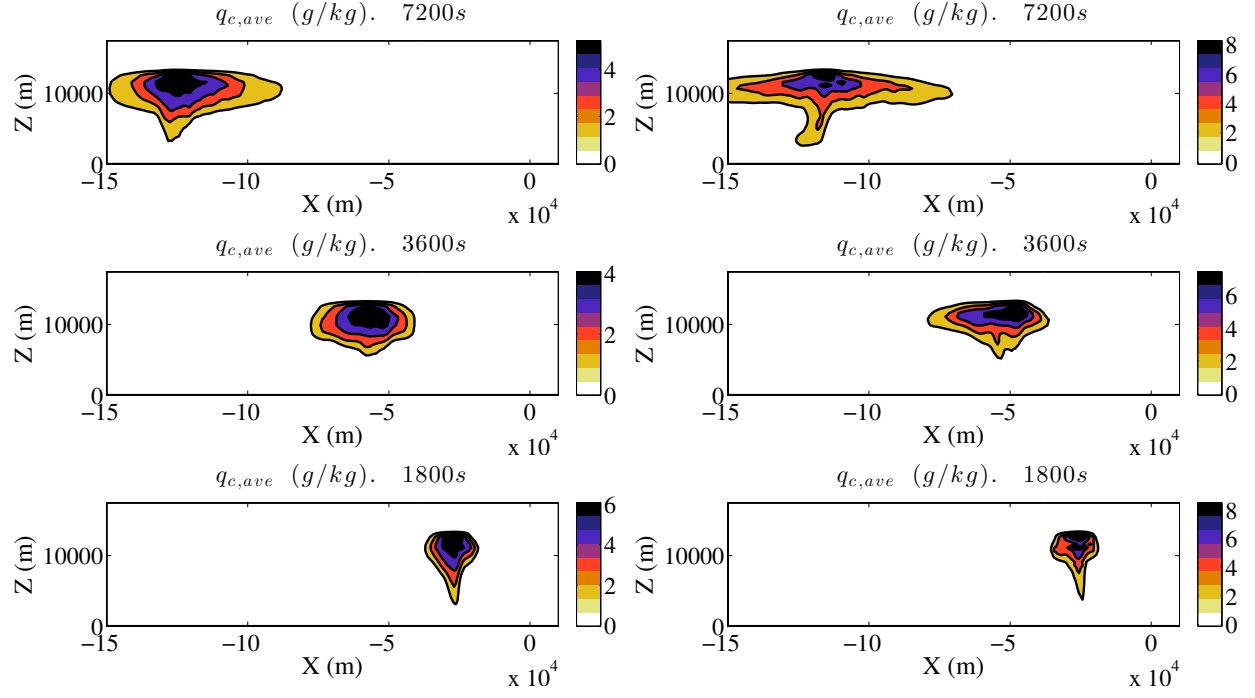


Figure 11: FM06: line averaged vertical cross sections of q_c at 1800, 3600, and 7200 seconds. Stabilization achieved by VMS+DC (left column) and by HV with $\nu_4 = 1 \times 10^8 \text{ m}^4 \text{ s}^{-1}$ (right column).

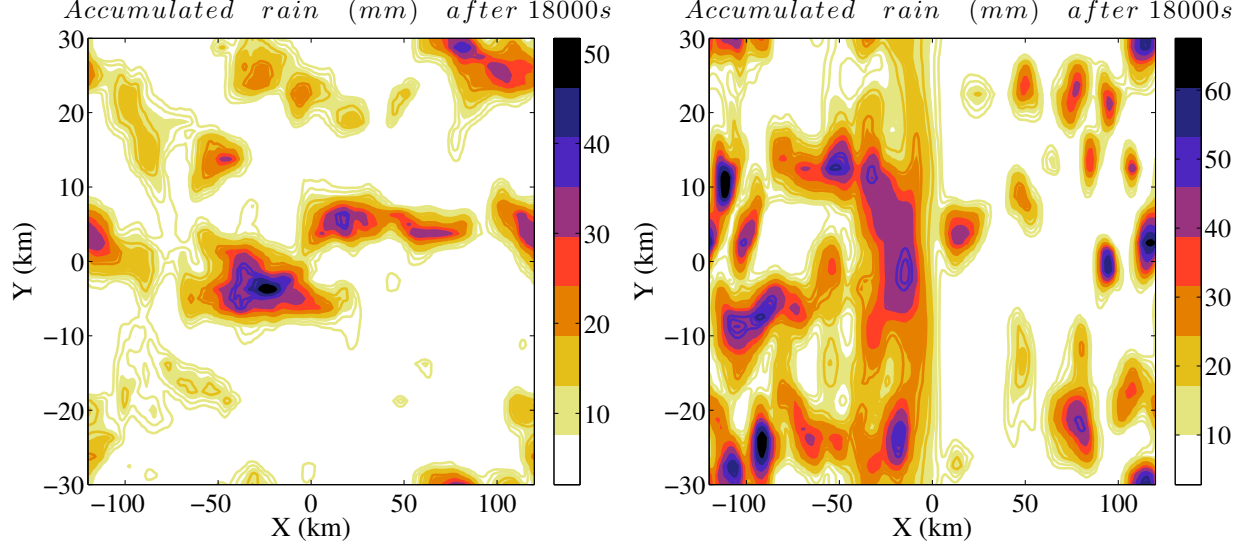


Figure 12: FM06: total accumulated rainfall (mm) at $t_f = 18000s$. Left: VMS+DC. Right: HV_a with $\nu_x = \nu_y = 1 \times 10^9 \text{ m}^4 \text{ s}^{-1}$, $\nu_z = 3 \times 10^5 \text{ m}^4 \text{ s}^{-1}$.

Table 2: Salient properties of VMS+DC and HV

Method	Parameter-free	Anisotropic	Consistent	Monotonicity	Parallel communication
VMS + DC	✓	✓	✓	Improved	As ∇^2
HV	×	✓	✓	×	As $\nabla^{2\alpha}$

and DC than by high order dissipative operators. As we try to approach the exascale range of computing, fewer communications are essential for faster and more scalable codes. We summarize the most salient properties of VMS+DC in Table 2.

Although the method hereby described was originally designed around a second order operator, we do not foresee a reason why, by a dimensionally consistent correction, it could not be adapted for higher order operators in case one were interested in extending this machinery to a parameter-free higher order hyper-viscosity-like dissipation. In this case, however, the cost of parallel communication would increase.

Finally, although it was built for finite and spectral elements, the discontinuity capturing dissipation DC could be constructed, with little effort, for alternative numerical techniques such as finite volume and finite difference methods.

5. Acknowledgments

The authors are thankful to Dr. Hilary Weller (U. Reading, UK), Dr. Guillaume Houzeaux (Barcelona Supercomputing Center, Spain), and one anonymous reviewer for important inputs that helped improve this article. The authors gratefully acknowledge the support of the Office of Naval Research through program element PE- 0602435N, the National Science Foundation (Division of Mathematical Sciences) through program element 121670. The work of the first author was carried out through the National Research Council (NRC) Research Associateship Programs.

6. Bibliography

- C. Jablonowski, D. L. Williamson, The pros and cons of diffusion, filters and fixers in atmospheric general circulation models, in: P. H. Lauritzen, C. Jablonowski, M. A. Taylor, R. D. Nair (Eds.), *Numerical Techniques for Global Atmospheric Models*, vol. 80 of *Lecture notes in computational science and engineering*, Springer, 381–482, 2011.
- G. Baruzzi, W. Habashi, N. Hefez, A second order accurate finite element method for the solutions of the Euler and Navier-Stokes equations, in: *Proceedings of the 13th International Conference on Numerical Methods in Fluid Dynamics*, Rome. Springer, 509–513, 1992.
- R. Codina, Stabilized finite element approximation of transient incompressible flows using orthogonal subscales, *Comput. Methods Appl. Mech. Engrg.* 191 (2002) 4295–4321.
- T. J. R. Hughes, A. N. Brooks, A multidimensional upwind scheme with no crosswind diffusion, in: T. J. R. Hughes (Ed.), *Finite element methods for convection dominated flows*, ASME, vol. 32, 19–35, 1979.
- T. J. R. Hughes, M. Mallet, A. Mizukami, A new finite element formulation for computational fluid dynamics: II. Beyond SUPG, *Comp. Methods Appl. Mech. Engrg.* 54 (1986) 341–355.
- R. Codina, A discontinuity-capturing crosswind-dissipation for the finite element solution of the convection-diffusion equation, *Comput. Methods Appl. Mech. and Engrg.* 110 (1993) 325–342.
- S. Marras, J. F. Kelly, F. X. Giraldo, M. Vázquez, Variational multiscale stabilization of high-order spectral elements for the advection-diffusion equation, *J. Comput. Phys.* 231 (2012) 7187–7213.
- H. Vandeven, Family of spectral filters for discontinuous problems, *J. Sci. Comp.* 159.
- J. P. Boyd, Two comments on filtering for Chebyshev and Legendre spectral and spectral element methods, *J. Comput. Phys.* 143 (1998) 283–288.
- J. Malm, P. Schlatter, P. F. Fischer, D. S. Henningson, Stabilization of the Spectral Element Method in Convection Dominated Flows by Recovery of Skew-Symmetry, *J. Sci. Comput.* 57 (2013) 254–277.

- T. Hughes, Multiscale phenomena: Green's functions, the Dirichlet-to-Neumann formulation, sub-grid scale models, bubbles and the origins of stabilized methods, *Comput. Methods Appl. Mech. and Engrg.* 127 (1995) 387–401.
- T. Gjesdal, C. E. Wasberg, B. A. P. Reif, Ø. Andreassen, Variational multiscale turbulence modelling in a high order spectral element method, *J. Comput. Phys.* 228 (2009) 7333–7356, ISSN 0021-9991.
- S. Marras, M. Moragues, M. R. Vázquez, O. Jorba, G. Houzeaux, Simulations of moist convection by a variational multiscale stabilized finite element method, *J. Comput. Phys.* 252 (2013) 195–218.
- J. F. Kelly, F. X. Giraldo, Continuous and discontinuous Galerkin methods for a scalable three-dimensional nonhydrostatic atmospheric model: limited-area mode, *J. Comput. Phys.* 231 (2012) 7988–8008.
- F. X. Giraldo, J. F. Kelly, E. Constantinescu, Implicit-explicit formulations of a three-dimensional Nonhydrostatic Unified Model of the Atmosphere (NUMA), *SIAM J. Sci. Comput.* 35 (2013) 1162–1194.
- G. I. Marchuk, *Numerical Methods in Weather Prediction*, Academic Press, 1974.
- E. Kessler, On the distribution and continuity of water substance in atmospheric circulation, *Meteorol. Monogr.* 10 (1969) 32.
- S. Soong, Y. Ogura, A comparison between axisymmetric and slab-symmetric cumulus cloud models, *J. Atmos. Sci.* 30 (1973) 879–893.
- P. Knobloch, On the definition of the SUPG parameter, *Electr. Trans. on Numer. Anal.* 32 (2008) 76–89.
- H. Owen, G. Houzeaux, C. Samaniego, A. C. Lesage, M. Vázquez, Recent ship hydrodynamics developments in the parallel two-fluid flow solver Alya, *Comput. Fluids* 80 (2013) 168–177.
- G. Houzeaux, B. Eguzkitza, M. Vázquez, A variational multiscale model for the advection-diffusion-reaction equation, *Comm. Numer. Meth. Engrg.* 25 (2009) 787–809.
- O. Guba, M. A. Taylor, P. A. Ullrich, J. R. Overfelt, M. N. Levy, The spectral element method on variable resolution grids: evaluating grid sensitivity and resolution-aware numerical viscosity, *Geosci. Model Dev.* 7 (2014) 4081–4117.
- M. L. Weisman, J. B. Klemp, R. Rotunno, Structure and evolution of numerically simulated squall lines, *J. Atmos. Sci.* 45 (1988) 1990–2013.

- J. Frame, P. Markowski, The interaction of simulated squall lines with idealized mountain ridges, Mon. Wea. Rev. 134 (2006) 1919–1941.
- M. L. Weisman, J. B. Klemp, The dependence of numerically simulated convective storms on vertical wind shear and buoyancy, Mon. Wea. Rev. 110 (1982) 504–520.
- M. L. Weisman, R. Rotunno, "A theory for strong long-lived squall lines" revisited, J. Atmo. Sci. 61 (2004) 361–382.